JOURNAL OF MATERIALS SCIENCE 22 (1987) 4125–4132

Effect of dopant concentration on electrical conductivity in the Sc_2O_3–ZrO_2 system

S. P. S. BADWAL
CSIRO, Division of Materials Science and Technology, Normanby Road, Clayton, Victoria, Australia 3168

Electrical conductivity measurements have been made as a function of dopant concentration (4 to 8 mol % Sc_2O_3) in the scandia–zirconia system. All the compositions studied had a tetragonal structure. The rhombohedral β phase was present only in samples prepared from mechanical mixtures of Sc_2O_3 and ZrO_2. In specimens prepared by coprecipitation, no β phase lines were observed and the monoclinic zirconia (m-ZrO_2) phase was present for only Sc_2O_3 contents $\leqslant 5$ mol %. The conductivity of Sc_2O_3–ZrO_2 decreased continuously with time up to 300 h anneal time between 700 and 1000° C. X-ray diffraction of coprecipitated specimens of 7.8 mol % Sc_2O_3–ZrO_2 composition annealed at 1000° C (28 days), 750° C (42 days) or 460° C (189 days) did not reveal any changes to account for this. However, transmission electron microscopy showed that changes associated with the formation of very fine precipitates had occurred. The activation energy for conduction in the low-temperature region decreased monotonically with decrease in the scandia content. Jumps in the conductivity curves and hysterisis effects were observed in specimens containing m-ZrO_2.

1. Introduction

Scandia–zirconia fluorite-related solid solutions have been known for sometime to have the highest conductivity amongst zirconia-based electrolytes [1, 2]. The best conductivity in the 800 to 1000° C temperature range occurs for scandia content around 8 to 9 mol % [3, 4]. These compositions have the fluorite-related structure [3, 5, 6] which is close to face-centred cubic symmetry. In compositions below about 6 to 7 mol % Sc_2O_3, monoclinic zirconia (m-ZrO_2) coexists with this fluorite-related phase [7, 8] while for Sc_2O_3 content of 8 mol % or above, the presence of an ordered rhombohedral phase (the β phase) has been reported [5, 6, 8–11]. The ideal composition of the β phase has been variously given as 12.5 mol %. Sc_2O_3 [3] and as 12.73 mol % Sc_2O_3 [9]. Thornber *et al.* [9] published a phase diagram constructed on the basis of their own work and that of others (see [9]). The more recent diagram of Ruh *et al.* [6] differs markedly from that of Thornber *et al.* especially in the zirconia-rich region. According to the latter phase diagram, the β phase exists over a composition range ($\sim$ 10 to 13 mol % Sc_2O_3) whereas Thornber *et al.* have shown it as a line phase (12.73 mol % Sc_2O_3). Moghadam *et al.* [11] have reported the existence of β phase in 8 mol % Sc_2O_3–ZrO_2 composition; a significantly lower scandia concentration according to both phase diagrams. These discrepancies may arise from the difficulty in obtaining equilibrium in the Sc_2O_3–ZrO_2 system as noted by Thornber *et al.* [9].

Irrespective of the equilibrium situation the presence of both m-ZrO_2 and β phases have a detrimental effect on the conductivity of scandia–zirconia electrolytes [3, 8, 10, 12, 13].

Some authors have also reported a decrease in the conductivity of 8 to 9 mol % Sc_2O_3–ZrO_2 compositions with time [11, 13]. Their results were interpreted in terms of precipitation of the low conducting β phase. Because most of the reported conductivity data [4, 8, 13, 14] are on specimens prepared by mixing the pure oxides, inhomogeneities are likely to be present and there must be considerable uncertainty as to the nature of this ageing process. The specimen preparation techniques therefore, in addition to influencing the phase equilibrium, may also play a major role in determining the electrolyte conductivity.

In this paper we report results of conductivity measurements on several scandia–zirconia compositions (4 to 8 mol % Sc_2O_3) prepared both by mixed oxide and coprecipitation techniques. In addition, conductivity as a function of time has been studied on one composition at several temperatures.

2. Experimental procedures

The Sc_2O_3–ZrO_2 samples under study were in the 4 to 8 mol % Sc_2O_3 concentration range. Two techniques were used for preparing these compositions.

(i) Sc_2O_3 (AMDEL, > 99.5%) and ZrO_2 (Harshaw > 99.5%, containing 2 wt % HfO_2) powders of the required composition were mixed thoroughly using water as the mixing media. The powder was dried, calcined at 1100° C (1 h), pressed into bar shapes and sintered at 1700° C (15 h). One bar of each composition was given a further heat treatment at 1900° C (3 h) in a gas-fired furnace.

(ii) The scandium and zirconium hydroxides were coprecipitated by aqueous ammonia from a homogeneous solution, containing the required quantities of

0022–2461/87 $03.00 + .12

TABLE I Specimen preparation details, densities and m-ZrO_2 content

Sc_2O_3 in Sc_2O_3–ZrO_2 (mol %)	Sintering conditions, T (° C), (time, h)	Density ($g\,cm^{-3}$)	m-ZrO_2 (%)	Nomenclature
Coprecipitated specimens				
7.8	2000 (20)	5.5	0	A-1
7.0	1900 (7)	5.7	0	A-2
6.0	1900 (5.5)	5.7	0	A-3
5.0	1900 (5.5)	5.8	< 4	A-4
4.5	1900 (7)	5.8	8–10	A-5
4.0	1900 (7)	5.5	–	A-6
Mixed oxide specimens				
7.8	1700 (15)	–	12	B-1a
7.8	1700 (15), 1900 (3)	–	0	B-1b
6.8	1700 (15)	–	24	B-2a
6.8	1700 (15), 1900 (3)	–	6	B-2b
5.9	1700 (15)	–	30	B-3a
5.9	1700 (15), 1900 (3)	–	16	B-3b
4.9	1700 (15)	–	44	B-4a
4.9	1700 (15), 1900 (3)	–	25	B-4b
4.4	1700 (15)	–	47	B-5a

scandium and zirconium. The coprecipitated powder was calcined at temperatures ranging from 750 to 900° C for 1 to 2 h. The calcined powder was pressed into bar shapes which were then sintered directly at 1900° C (5 to 7 h) in a gas-fired furnace.

Table I gives details of sample preparation, sintering conditions, nomenclature and measured densities.

The microstructure of polished and etched samples was examined with both scanning electron and optical microscopy. X-ray diffraction analysis was performed with a diffractometer. A Hagg Guinier focusing camera was used for selected specimens. For indexing diffraction patterns of these samples, ThO_2 was used as the internal standard. The monoclinic zirconia (m-ZrO_2) content in the samples was determined by the integrated intensity method reported by Garvie and Nicholson [15]. Thermal expansion curves for some m-ZrO_2 containing samples were recorded with a modified Gebruder Netzsche dilatometer.

Conductivity measurements on all the specimens were made with a four-probe d.c. technique over the temperature range 350 to 1000° C for several heating and cooling cycles [16]. After the specimens were taken to 1000° C during the first heating cycle they were annealed at that temperature for 20 to 100 h during which time the conductivity was recorded intermittently. Impedance measurements were made on selected specimens to determine the grain-boundary resistivity over the temperature and frequency ranges of 350 to 600° C and 1 Hz to 1 MHz, respectively.

In order to understand the ageing process, two types of experiments were performed. In the first, coprecipitated and presintered specimens of 7.8 mol % Sc_2O_3–ZrO_2 composition were annealed at 1000° C (28 days), 750° C (42 days) or 460° C (189 days). The specimens, after annealing, were subjected to X-ray and transmission electron microscopic (TEM) analysis. For TEM work specimens were ion-beam thinned. In the second set of experiments which took more than 100 days to complete, the conductivity (four-probe d.c.) was measured as a function of time at temperature, T_m (T_m = 1000, 900, 800 or 700° C) on a single coprecipitated specimen of 7.8 mol % Sc_2O_3–ZrO_2 composition. Each time-dependent conductivity measurement experiment involved the following steps:

(i) heat treating the presintered specimen at 1700° C (15 h) in air except for the first experiment for which freshly sintered sample was used;

(ii) assembling the sample in the conductivity rig;

(iii) heating the specimen slowly and recording conductivity data at 25 to 50° C temperature intervals between 450° C and T_m;

(iv) holding the temperature at T_m for 280 to 350 h while measuring the conductivity at regular time intervals, and

(v) slowly cooling the specimen and recording data at 25° C temperature intervals between T_m and 400° C.

This procedure (i–v) was repeated twice for T_m = 1000° C and once for T_m of 900, 800 and 700° C.

3. Results and discussion

3.1. Characterization

3.1.1. Mixed oxide specimens

All specimens prepared by mixing oxides after the 1700° C sintering contained m-ZrO_2 which increased rapidly with decreasing Sc_2O_3 concentration. On heating to 1900° C the m-ZrO_2 lines disappeared in a sample of 7.8 mol % Sc_2O_3–ZrO_2 composition. In all other specimens a significant decrease in the m-ZrO_2 content was observed (Table I). Examination of the sintered specimens with an optical microscope showed several cracks, most of which originated from m-ZrO_2 grains (Fig. 1). The cracks increased in size and density with increasing m-ZrO_2 content and also on thermal cycling. Fig. 2 shows the microstructure of some mixed oxide specimens. The twinned regions in Figs 1 and 2 are associated with the presence of m-ZrO_2. These regions had a lower Sc_2O_3 concentration compared with that in the untwinned grains. X-ray diffractograms of the mixed oxide specimens also showed the presence of the β phase for Sc_2O_3 concentrations $\geqslant$ 5 mol % even after the 1900° C heat treatment. The relative intensity of β phase lines decreased with

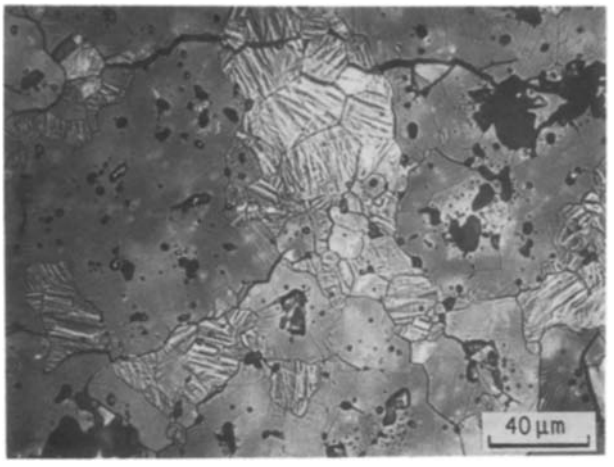

Figure 1 Optical micrograph of a mixed oxide specimen of 5.9 mol % Sc_2O_3–ZrO_2 composition (B-3b). Twinned regions are m-ZrO_2 grains.

decreasing scandia content. Crushing, grinding, repelleting and refiring (1900° C) a 7.8 mol % Sc_2O_3–ZrO_2 composition, containing the largest amount of β phase, resulted in its complete disappearance. These observations, combined with the phase diagram evidence [6, 9] clearly indicate that higher Sc_2O_3 concentrations are required for the formation of this phase, and that its presence in compositions containing 8 mol % (or less) Sc_2O_3 is associated with micro-inhomogeneities in the mixed oxide samples.

3.1.2. Coprecipitated specimens

In the coprecipitated specimens in which the distribution of scandium and zirconium is inherently more uniform, the m-ZrO_2 lines appeared only for Sc_2O_3 concentrations of 5 mol % or less. The 4.5 mol % Sc_2O_3–ZrO_2 specimen contained only 8 to 10% m-ZrO_2 consistent with the results of Bannister and Skilton [5]. Microcracks were observed only in the 4 mol % Sc_2O_3–ZrO_3 composition. Fig. 3 shows the microstructure of some etched specimens. The average grain size is more than 20 to 30 μm and no impurity phases were detected in the grain boundaries or at triple points by either scanning or transmission electron microscopes. Twinned regions were observed only in the 4 and 4.5 mol % Sc_2O_3–ZrO_2 compositions. The fluorite-related phase in the as-sintered (not annealed) specimens could be indexed as tetragonal (t_{sc}). This phase probably is the distorted tetragonal phase (α'_2) of Ruh *et al.* [6].

No β-phase lines were detected even in the 7.8 mol % Sc_2O_3–ZrO_2 composition. X-ray diffraction on annealed [1000° C (28 days), 750° C (42 days) or 460° C (27 weeks)] specimens also did not show the precipitation of the β phase. However, changes in the grain structure could be observed by transmission electron microscopy. In materials which had not been subjected to any ageing, the grain structure consisted of lamellae of varying width (Fig. 4a). Electron diffraction from these regions indicated that the material was a single phase of tetragonal symmetry (t_{sc}) and the individual lamellae simply represented twins of different orientation. No compositional differences could be observed from one twin to another. Also no evidence was found for the existence of the β phase.

Alternatively, materials which had been aged did not have this structure. The individual grains showed a mottled appearance (Fig. 4b) somewhat similar to the types of microstructures observed for the Y_2O_3–ZrO_2 system (Fig. 7 in [17]). Electron diffraction once again indicated mainly tetragonal symmetry. However, in addition, some diffuse scatter similar to that reported by Rossell [18] was also clearly evident. We suggest that the microstructure now consists of tetragonal zirconia (t) precipitates (estimated to be ~ 10 to 30 nm in size from dark-field image) coherently

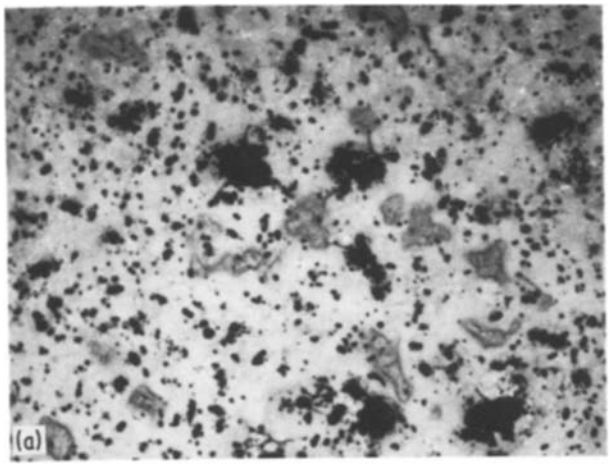

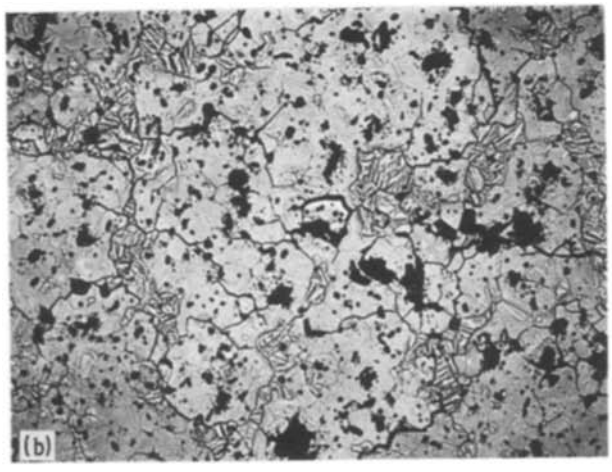

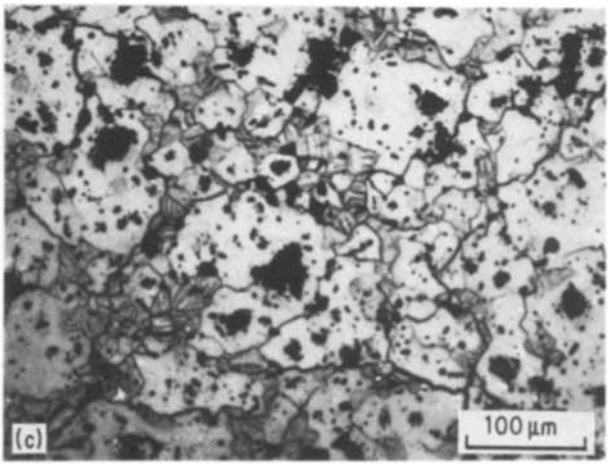

Figure 2 Microstructure of mixed oxide specimens. (a) 6.8 mol % Sc_2O_3–ZrO_2 (B-2b), (b) 5.9 mol % Sc_2O_3–ZrO_2 (B-3b), (c) 4.9 mol % Sc_2O_3–ZrO_2 (B-4b).

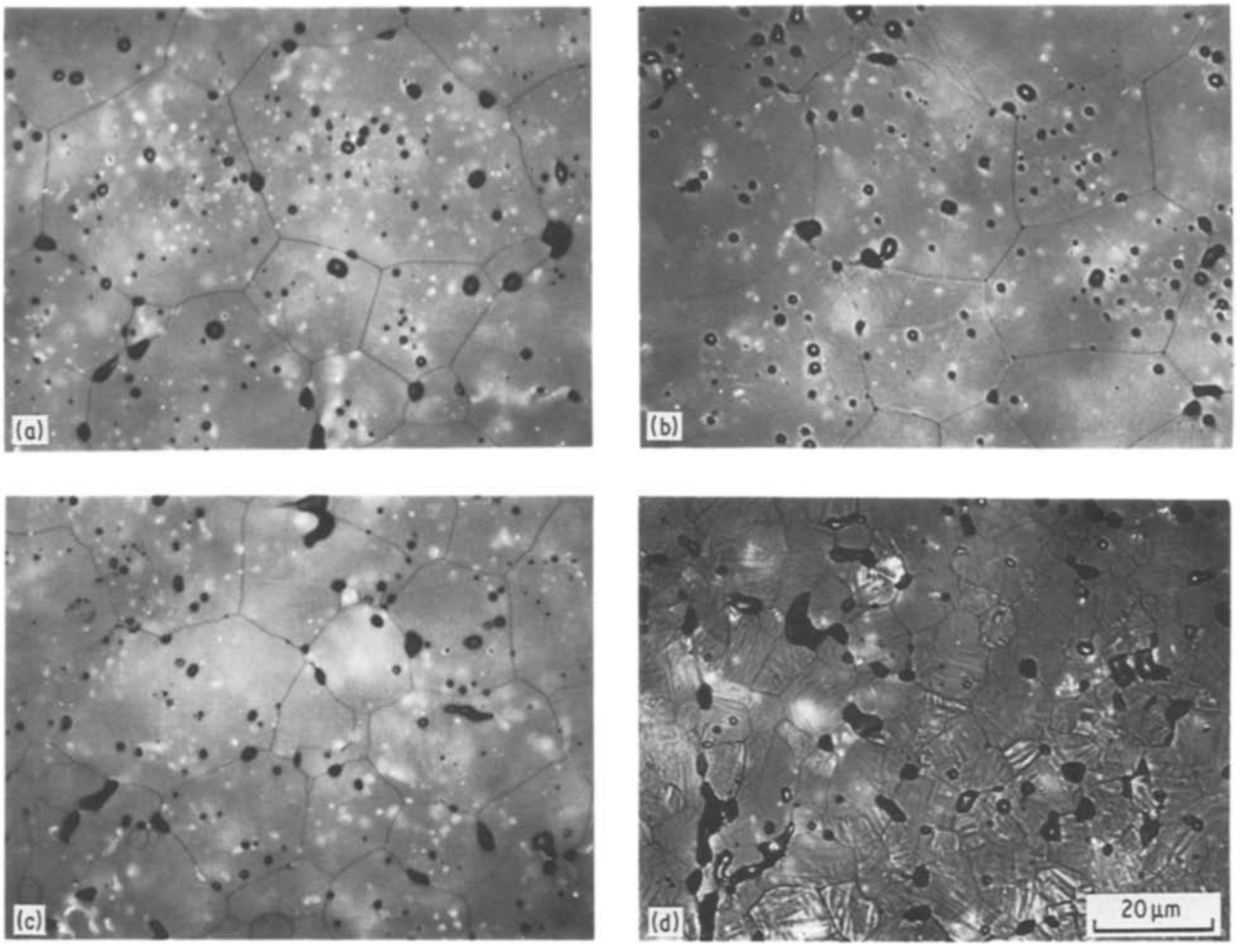

Figure 3 Microstructure of coprecipitated specimens. (a) 7 mol % Sc_2O_3–ZrO_2 (A-2), (b) 6 mol % Sc_2O_3–ZrO_2 (A-3), (c) 4.5 mol % Sc_2O_3–ZrO_2 (A-5), (d) 4.0 mol % Sc_2O_3–ZrO_2 (A-6).

grown in the surrounding scandia-rich tetragonal matrix (t_{sc}). The diffuse scatter may have resulted from the growth of δ or even γ phase [6] at the t/t_{sc} interfaces. This type of phenomenon has been reported by Hannink in the magnesia–zirconia system [19].

These results are in sharp contrast to those reported by Moghadam *et al.* [11] on a specimen of 8 mol % Sc_2O_3–ZrO_2 composition. These authors found about 5% rhombohedral β phase in the as-received specimens (from Applied Electrochemistry Corp., Sunnyvale, California, USA) which after the 800° C anneal for 200 h increased to 10 to 15%. This rapid precipitation of β phase in their specimen may be a consequence of inhomogeneous distribution of scandium and zirconium.

3.2. Conductivity

3.2.1. Effect of m-ZrO_2 and β phases

Arrhenius curves of all mixed oxide specimens except the 7.8 mol % Sc_2O_3–ZrO_2 composition heated at

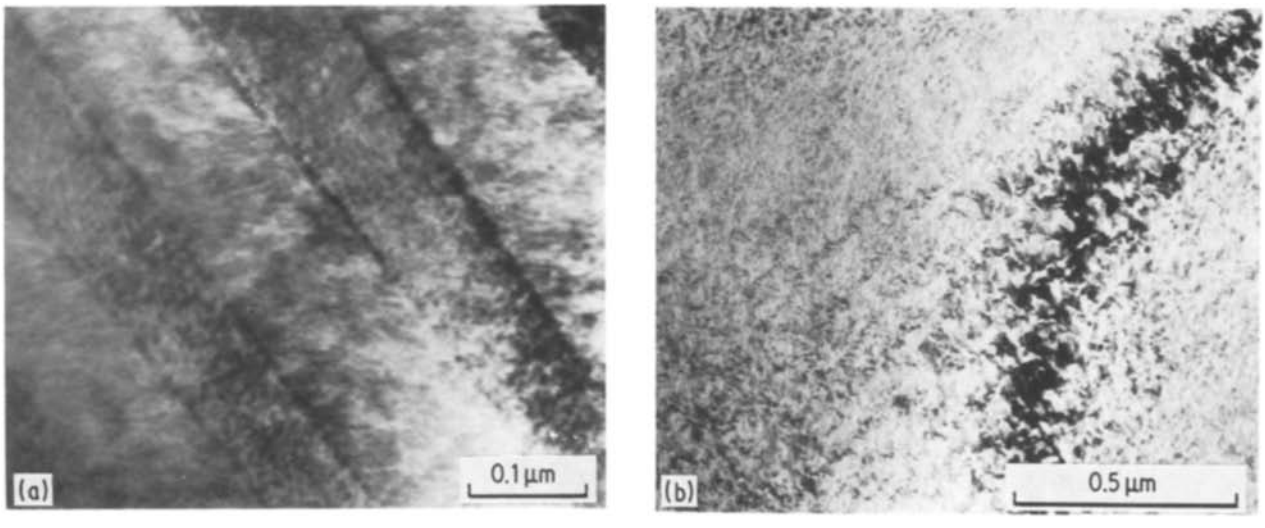

Figure 4 Transmission electron micrographs of 7.8 mol % Sc_2O_3–ZrO_2, (a) freshly sintered, (b) after anneal at 1000° C for 28 days.

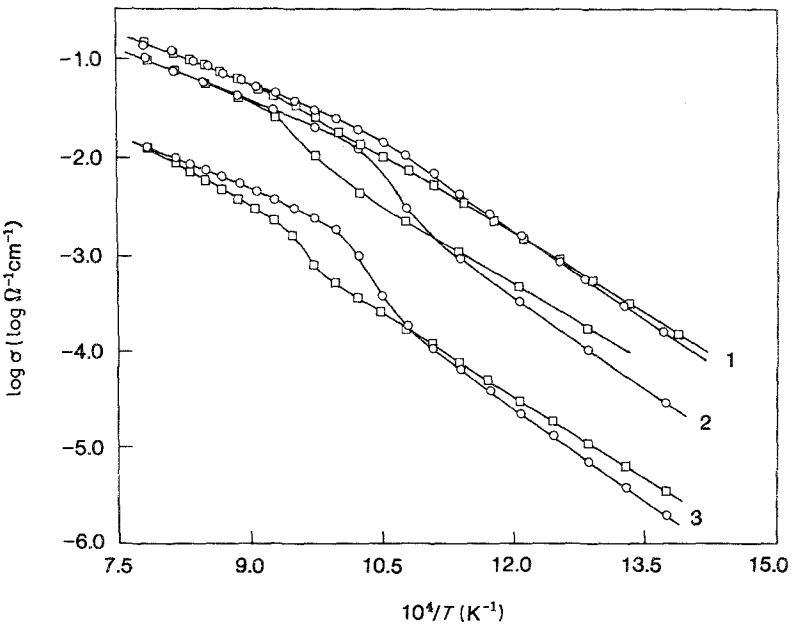

Figure 5 Arrhenius plots for mixed oxide samples. (1) B-2b, (2) B-3b, (3) B-4b. (□) Heating, (○) cooling cycle.

1900° C showed distinct jumps and hysteresis loops (Fig. 5). The size of the jump and hysteresis loop decreased with decreasing m-ZrO_2 content in the specimens (Fig. 6). Amongst coprecipitated samples only the 4 mol % Sc_2O_3–ZrO_2 composition showed hysteresis effects during thermal cycling (Fig. 7). The temperature range of the hysteresis loop coincided with that of the m-$ZrO_2 \rightleftharpoons$ *t*-ZrO_2 (tetragonal zirconia) transformation, determined by thermal expansion. The conductivity of m-ZrO_2-containing specimens also deteriorated with thermal cycling. This effect appears to be caused by the observed increase in the crack density in specimens cycled through the m-$ZrO_2 \rightleftharpoons$ *t*-ZrO_2 transformation.

The presence of a small quantity of β phase in the mixed oxide specimens did not appear to have an effect on the shape of the Arrhenius plots.

3.2.2. Effect of time on conductivity

The conductivity of all scandia–zirconia specimens decreased with time at 1000° C irrespective of the presence or absence of m-ZrO_2 and/or the β phases. In specimens free of these phases, the conductivity decreased by about 30 to 40% over a period of 100 to 150 h. In order to further explore this phenomenon, conductivity measurements as a function of time were made on a coprecipitated specimen of 7.8 mol % Sc_2O_3–ZrO_2 composition at 1000, 900, 800 and 700° C as described earlier. This specimen was free of m-ZrO_2 and the β phases. Fig. 8 shows conductivity–time plots at 800 and 1000° C. The conductivity decreased rapidly in the first 80 to 100 h and then more slowly. The second conductivity–time curve recorded at T_m of 1000° C, after the specimen had been heat-treated at 1700° C (15 h), overlapped with the first where the specimen had been cooled directly after sintering at 2000° C (Fig. 8). The rate of conductivity change was a maximum at 900° C. The Arrhenius plots for the heating portion of all cycles overlapped. Fig. 9 shows plots for the heating cycles of second (T_m = 1000° C) and the last (T_m = 700° C) conductivity–time experiment. These results clearly indicate that (i) the effect of ageing can be readily reversed on heat treating the specimen at 1700° C, and (ii) the ageing process is slow and extremely reproducible. In the high-temperature region (800 to 1000° C) the activation energy was

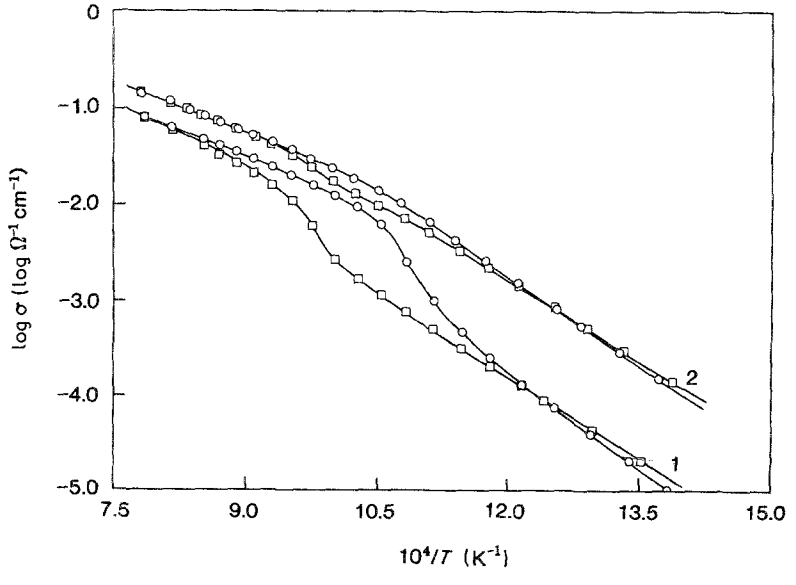

Figure 6 Arrhenius plots for a mixed oxide specimen of 6.8 mol % Sc_2O_3–ZrO_2 composition showing a decrease in the size of the hysteresis loop with decreasing m-ZrO_2 content. (1) B-2a, (2) B-2b. (□) Heating, (○) cooling cycle.

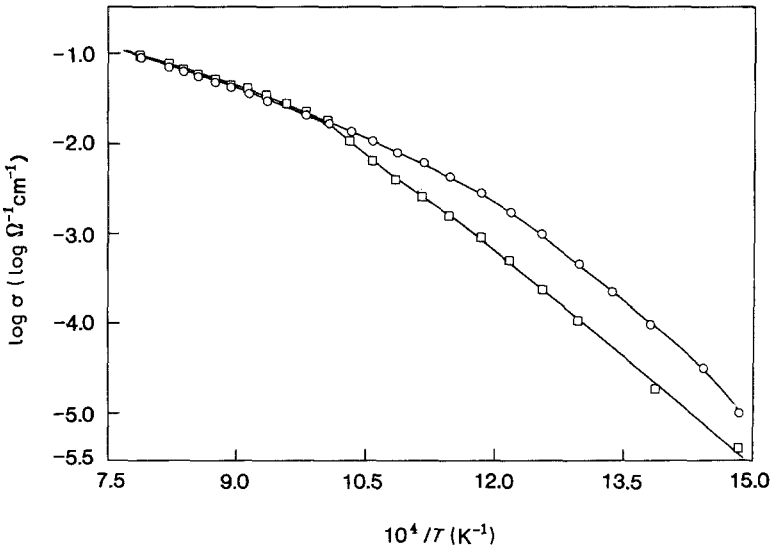

Figure 7 Arrhenius plots for a coprecipitated specimen of 4.0 mol % Sc_2O_3–ZrO_2 composition. (□) Heating, (○) cooling cycle.

higher by 8 to 10 kJ mol^{-1} for the cooling cycle (step v) compared with that for the heating cycle (step iii). In the low-temperature (400 to 500° C) region no significant differences were observed.

The kinetics of the observed ageing process is such that it cannot be assigned to a martensitic-type transformation. X-ray and TEM analysis on a specimen from the same lot heat treated at 1000° C for 28 days (a period much longer than that over which conductivity–time curves were recorded) did not show the presence of the β phase. The large decrease in the conductivity with time, therefore, is unlikely to be due to the precipitation of the less conducting β phase. The exact nature of the ageing process is not clear at this stage and further work is in progress. Nevertheless, the TEM evidence previously described suggests that the decrease in the conductivity may be associated with disproportionation of the tetragonal phase of the as-sintered specimens. The subtle compositional changes required in disproportionation may occur only slowly in mixtures as intimate as those produced by coprecipitation. Moreover, because of the intrinsic slowness of phase reactions in the Sc_2O_3–ZrO_2 system compared with other systems it is likely that the products of decomposition are themselves metastable and may not be represented on the equilibrium phase diagram.

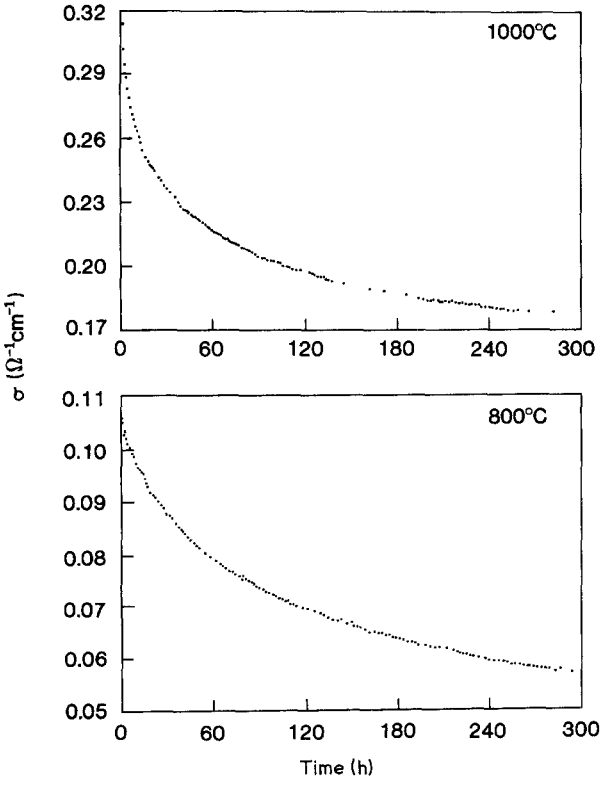

Figure 8 Conductivity–time plots at 800 and 1000° C for a coprecipitated specimen of 7.8 mol % Sc_2O_3–ZrO_2 composition.

3.2.3. Effect of temperature

Impedance measurements made on several coprecipitated specimens showed a very small contribution (about 10 to 15% of the total) from grain-boundary resistivity (Fig. 10). Also the activation energy for the lattice conductivity was similar to that for the total conductivity over the temperature range 400 to 600° C. These results are not surprising considering the large grain size of the specimens and the fact that they were free of impurities.

All the coprecipitated and mixed oxide specimens free of m-ZrO_2 showed a change in the slope of the Arrhenius plots around 600° C towards lower activation energy as the temperature increased. This behaviour was reproducible for all the heating and cooling cycles over which the four-probe d.c. data were recorded. The change in the slope was maximum for the 7.8 mol % Sc_2O_3–ZrO_2 composition and it decreased with decreasing scandia content. At 1000° C the best conductivity was observed for 7.8 mol % Sc_2O_3–ZrO_2 composition but at 400° C the 5 mol % Sc_2O_3–ZrO_2 specimen had the highest conductivity.

TABLE II Activation energies for coprecipitated specimens

Sc_2O_3 in Sc_2O_3–ZrO_2 (mol %)	Activation energy* l(kJ mol^{-1} ± 3 kJ mol^{-1})	
	H_m	H_σ
7.8	69	137
7.0	66	124
6.0	63	119
5.0	66	112
4.5	61	109

*Average of several heating and cooling cycles.

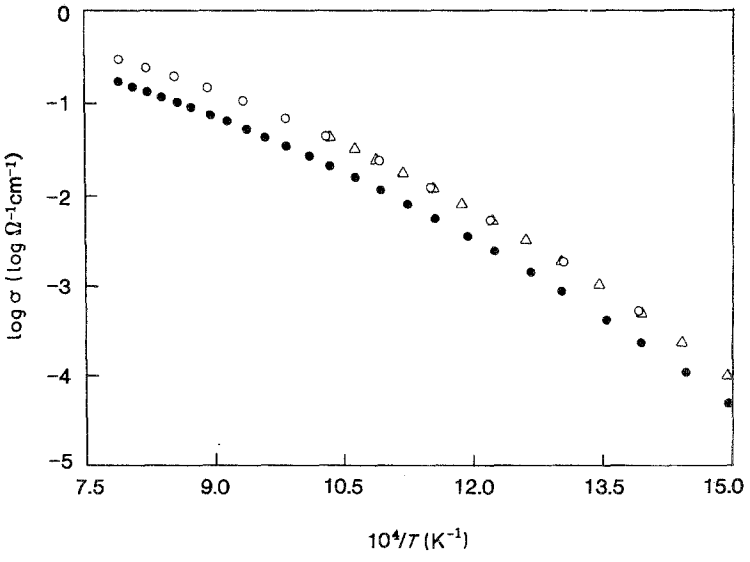

Figure 9 Arrhenius plots for the heating cycles from (○) 450 to 1000° C and (△) 400 to 700° C before recording conductivity–time plots at 1000 and 700° C, respectively. (●) Cooling cycle data obtained after recording conductivity–time data at 1000° C.

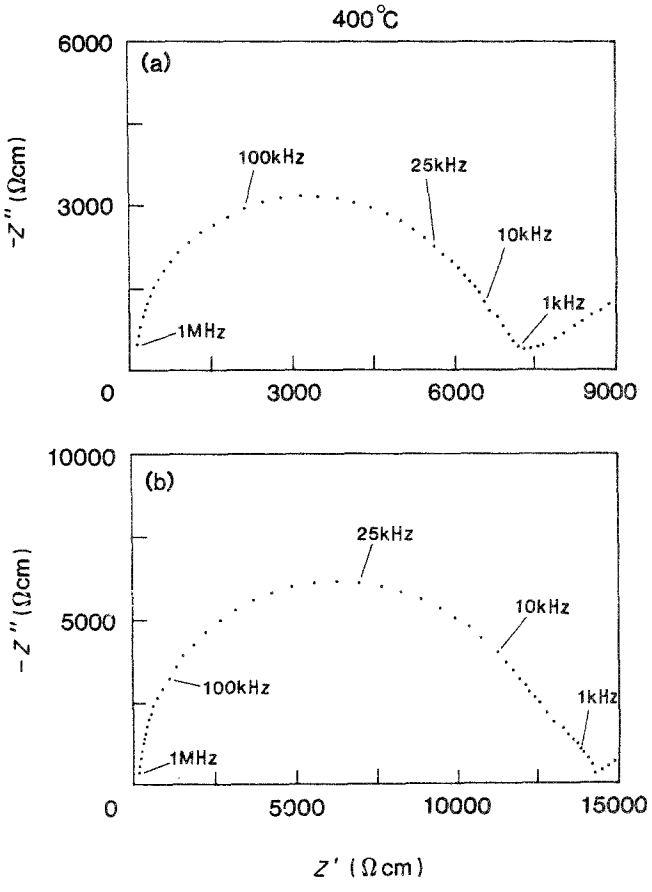

Figure 10 Impedance plots at 400° C for two coprecipitated specimens showing the electrolyte behaviour. (a) A-4, (b) A-2.

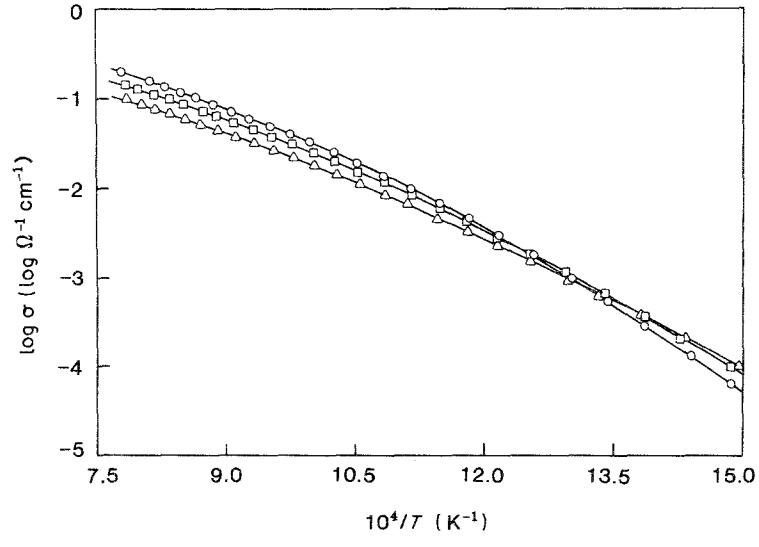

Figure 11 Arrhenius plots for coprecipitated specimens. (○) A-1, (□) A-3, (△) A-5.

Fig. 11 shows Arrhenius plots for some coprecipitated specimens.

In view of the small contribution from the grain-boundary resistivity, four-probe d.c. data can be considered to be reasonably representative of the lattice conductivity for coprecipitated specimens.

The change in the slope of the Arrhenius plots towards higher activation energy at low temperature appears to be due to the formation of dopant cation–vacancy complexes [20–22]. In order to determine the activation energies for the conduction processes dominating at the high and the low temperatures, the data were fitted to the following relationship [23]:

$$\varrho = A_1 T \exp(H_m/RT) + A_2 T \exp(H_\sigma/RT)$$

where H_m is the enthalpy of vacancy migration and H_σ consists of contributions from enthalpy of vacancy migration and enthalpy of association between dopant cations and vacancies. Table II gives values for H_m and H_σ for various coprecipitated specimens. The values of H_m do not change significantly but those of H_σ decrease monotonically with decrease in the scandia concentration. From these results it appears that the binding energy for defect interactions is much higher in the scandia–zirconia system compared with that in yttria–zirconia fluorite-type solid solutions [21, 23]. The reverse of this is true for the enthalpy of vacancy migration.

4. Conclusion

Because of the difficulty in achieving equilibrium in the scandia–zirconia system it is almost impossible to avoid inhomogeneities in the mixed oxide samples. The conductivity of scandia–zirconia compositions with the fluorite-related structure decreased continuously with time at temperatures between 700 and 1000° C. This behaviour in coprecipitated specimens does not appear to be a direct consequence of the precipitation of the low conducting β phase. In fact the kinetics of the process and preliminary TEM work suggests that the decrease in conductivity with time may be due to slow disproportionation of the tetragonal phase and perhaps some short-range ordering of the matrix. The change in the slope of Arrhenius plots around 600° C towards higher activation energy at lower temperatures indicates the formation of dopant cation–vacancy complexes with binding energy much higher than that in the yttria–zirconia fluorite-type solid solutions.

Acknowledgements

The author thanks B. Terrell, F. Ciacchi and R. Stringer for their assistance with the specimen preparation, Dr J. Drennan for TEM analysis, and Dr M. J. Bannister, Dr J. Drennan, Mr W. G. Garrett and Emeritus Professor D. J. M. Bevan for many useful discussions. The manuscript was kindly reviewed by Mr W. G. Garrett.

References

1. T. H.ETSELL and S. N. FLENGAS, *Chem. Rev.* **70** (1970) 339.
2. J. M. DIXON, L. D. LaGRANGE, V. MERTEN, C. F. MILLER and J. T. PORTER II, *J. Electrochem. Soc.* **110** (1963) 276.
3. F. M. SPIRIDONOV, L. N. POPOVA and R. Ya. POPIL'SKII, *J. Solid State Chem.* **2** (1970) 430.
4. D. W. STRICKLER and W. G. CARLSON, *J. Amer. Ceram. Soc.* **48** (1965) 286.
5. M. J. BANNISTER and P. F. SKILTON, *J. Mater. Sci. Lett.* **2** (1983) 561.
6. R. RUH, H. J. GARRETT, R. F. DOMAGALA and V. A. PATEL, *J. Amer. Ceram. Soc.* **60** (1977) 399.
7. P. DUWEZ, F. H. BROWN Jr and F. ODELL, *J. Electrochem. Soc.* **98** (1951) 356.
8. Z. S. VOLCHENKOVA and V. M. NEDOPEKIN, *IZV. Akad. Nauk. SSSR, Neorg. Mater.* **10** (1974) 1821.
9. M. R. THORNBER, D. J. M. BEVAN and E. SUMMERVILLE, *J. Solid State Chem.* **1** (1970) 545.
10. L. S. ALEKSEENKO, A. M. GAVRISH, N. V. GUL'KO, G. P. OREKHOVA, L. A. TARASOV and N. K. POLNITSKAYA, *Russ. J. Inorg. Chem.* **26** (4) (1981) 476.
11. F. K. MOGHADAM, T. YAMASHITA, R. SINCLAIR and D. A. STEVENSON, *J. Amer. Ceram. Soc.* **66** (3) (1983) 213.
12. S. P. S. BADWAL, *J. Mater. Sci.* **18** (1983) 3230.
13. M. V. INOZEMTSEV, M. V. PERFILEV and V. P. GORELOV, *Sov. Electrochem.* **12** (1976) 1128.
14. T. M. GUR, I. D. RAISTRICK and R. A. HUGGINS, *Mater. Sci. Engng* **46** (1980) 53.
15. R. C. GARVIE and P. S. NICHOLSON, *J. Amer. Ceram. Soc.* **55** (1972) 303.
16. S. P. S. BADWAL, *J. Mater. Sci.* **18** (1983) 3117.
17. M. RUHLE, N. CLAUSSEN and A. H. HEUER, "Advances in Ceramics", Vol 12, edited by N. Claussen, M. Ruhle and A. H. Heuer (The American Ceramic Society, Columbus, Ohio, 1984) p. 352.
18. H. J. ROSSELL, "Advances in Ceramics", Vol 3, edited by A. H. Heuer and L. W. Hobbs (The American Ceramic Soc., Columbus, Ohio, 1981) p. 47.
19. R. H. J. HANNINK, *J. Mater. Sci.* **18** (1983) 457.
20. J. A. KILNER and C. D. WATERS, *Solid State Ionics* **6** (1982) 253.
21. S. P. S. BADWAL, *J. Mater. Sci.* **19** (1984) 1767.
22. DA YU WANG, D. S. PARK, J. GRIFFITH and A. S. NOWICK, *Solid State Ionics* **2** (1981) 95.
23. S. P. S. BADWAL and M. V. SWAIN, *J. Mater. Sci. Lett.* **4** (1985) 487.

Received 2 February
and accepted 15 April 1987